Measured Performance of Building Integrated Photovoltaic Panels

By

A. Hunter Fanney, Brian P. Dougherty
And Mark W. Davis

National Institute of Standards and Technology
Building and Fire Research Laboratory
Heat Transfer and
Alternative Energy Systems Group
Gaithersburg, MD 20899-8632 USA

Reprinted from Transactions of the ASME, the Journal of Solar Energy Engineering, Special Issue: Solar Thermochemical Processing, Vol. 123, No.2, pp. 187-193, August 2001.

NIST
National Institute of Standards and Technology

Measured Performance of Building Integrated Photovoltaic Panels*

A. Hunter Fanney
e-mail: Hunter.Fanney@nist.gov

Brian P. Dougherty
e-mail: Brian.Dougherty@nist.gov

Mark W. Davis
e-mail: Mark.Davis@nist.gov

National Institute of Standards and Technology,
100 Bureau Drive, Stop 8632,
Gaithersburg, MD 20899-8632

The photovoltaic industry is experiencing rapid growth. Industry analysts project that photovoltaic sales will increase from their current $1.5 billion level to over $27 billion by 2020, representing an average growth rate of 25 %. (Cook et al. 2000) [1]. To date, the vast majority of sales have been for navigational signals, call boxes, telecommunication centers, consumer products, off-grid electrification projects, and small grid-interactive residential rooftop applications. Building integrated photovoltaics, the integration of photovoltaic cells into one or more of the exterior surfaces of the building envelope, represents a small but growing photovoltaic application. In order for building owners, designers, and architects to make informed economic decisions regarding the use of building integrated photovoltaics, accurate predictive tools and performance data are needed. A building integrated photovoltaic test bed has been constructed at the National Institute of Standards and Technology to provide the performance data needed for model validation. The facility incorporates four identical pairs of building integrated photovoltaic panels constructed using single-crystalline, polycrystalline, silicon film, and amorphous silicon photovoltaic cells. One panel of each identical pair is installed with thermal insulation attached to its rear surface. The second paired panel is installed without thermal insulation. This experimental configuration yields results that quantify the effect of elevated cell temperature on the panels' performance for different cell technologies. This paper presents the first set of experimental results from this facility. Comparisons are made between the electrical performance of the insulated and non-insulated panels for each of the four cell technologies. The monthly and overall conversion efficiencies for each cell technology are presented and the seasonal performance variations discussed. Daily efficiencies are presented for a selected month. Finally, plots of the power output and panel temperatures are presented and discussed for the single-crystalline and amorphous silicon panels. [DOI: 10.1115/1.1385824]

Introduction

More than two-thirds of the electricity in the United States is consumed by residential and commercial buildings [1]. The incorporation of photovoltaics into buildings, referred to as building integrated photovoltaics (BIPV), offers an aesthetically pleasing means of displacing centrally located utility generated power with distributed renewable energy. Building integrated photovoltaics replace conventional building elements such as roof tiles, asphalt shingles, façade elements, and shading devices with photovoltaic modules that perform the same functions but also provide electrical power.

In addition to concerns over first costs, a barrier to the wide spread proliferation of BIPV is the lack of performance data. A survey of 900 building professionals in the United Kingdom found that 88% would consider the use of integrated photovoltaic building products if there was greater evidence of the performance and reliability of these products [2]. Forty nine percent of the survey respondents noted that they would only consider building integrated products after they had seen them utilized in demonstration sites. Although a similar survey has not been conducted within the U.S., it is anticipated that the results would be comparable. An additional barrier to BIPV implementation is the lack of predictive performance tools to quantify the achievable energy savings. These predictive tools are needed by building owners, architects, and designers in order to make decisions concerning the economic viability of BIPV.

NIST's Building and Fire Research Laboratory hopes to accelerate the deployment of BIPV by addressing the need for performance data and validated performance models. A *test bed* located in Gaithersburg, MD, provides side-by-side comparisons of BIPV panels using different cell technologies and levels of thermal insulation. The resulting data will be compared to predictive models being developed by others including PVSIM [3], PHANTASM (PHotovoltaic ANalysis and TrAnsient Simulation Method) [4], ENERGY-10 [5], and IV Tracer [6].

Approach

NIST's Building Integrated Photovoltaic program is shown schematically in Fig. 1. The program consists of short-term testing to characterize the electrical performance of BIPV panels that utilize various cell technologies, modeling to predict the annual energy production of the characterized panels, and long-term performance monitoring of the BIPV panels under real world conditions.

In order to accurately predict the electrical output of BIPV systems, the panel's electrical response to various parameters must be known. The number of required electrical characteristics varies with the simulation model being used. For example, the model advocated by King [7] requires the following parameters:

- Influence of solar angle-of-incidence
- Influence of solar spectrum
- Temperature coefficients for the open circuit voltage and maximum power voltage

*This paper was presented at Forum 2001, *Solar Energy: The Power To Choose*, April 21–25, 2001, in Washington DC, where it received the Best Paper Award from the Photovoltaic Technical Committee.

Contributed by the Solar Energy Division of the THE AMERICAN SOCIETY OF MECHANICAL ENGINEERS for publication in the ASME JOURNAL OF SOLAR ENERGY ENGINEERING. Manuscript received by the ASME Solar Energy Division, November 2000; final revision, March 2001. Associate Editor: C. Vargas-Aburto.

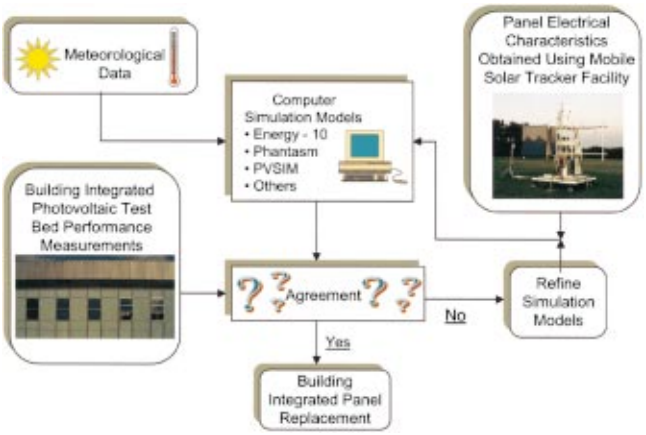

Fig. 1 NIST's Building Integrated Photovolatic Program

Fig. 2 Photovoltaic BIPV *Test Bed*

- Temperature coefficients for the short circuit current and the maximum power current
- Module operating temperature as a function of ambient temperature, wind velocity, and solar radiation

These parameters will be obtained from short-term tests using a mobile solar tracking facility [8]. The electrical characteristics obtained from the solar tracker and measured meteorological data will be supplied to simulation models. The predicted electrical energy produced by the various BIPV technologies will be compared to the measurements from NIST's BIPV *test bed*, the subject of this paper. In addition to providing validation data, the BIPV *test bed* will provide side-by-side comparisons of various cell technologies under real world conditions. Discrepancies between measured and modeled results will be reported to the authors of the simulation models. The end result will be predictive performance tools that can be used to confidently assess the energy savings potential of BIPV.

Building Integrated Photovoltaic Test Facility

A facility has been built to provide experimental data needed to validate and improve predictive performance tools for building integrated photovoltaic panels. This building integrated photovoltaic *test bed* is located on the south wall of NIST's Building Research building, Fig. 2. This facility was created by removing five adjacent windows and modifying the framing system to facilitate the installation and removal of building integrated photovoltaic panels. A moveable horizontal shelf partitions each opening into two test cells. Each panel's front surface is mounted as close to the front surface of the surrounding framework as possible in order to minimize shading.

The eight BIPV panels selected for the initial one-year study include custom-fabricated single-crystalline, polycrystalline, and silicon film panels and commercially available amorphous silicon modules. Specifications for each panel are given in Table 1. Two identical custom fabricated panels are installed, one above the other, in six of the test cells. Tandem, commercially available, amorphous silicon modules are installed in the upper area of two openings. The lower areas of these two openings are allocated to meteorological instrumentation and a building integrated photovoltaic panel used exclusively for heat flux measurements. Extruded polystyrene insulation, having a thickness of 10.2 cm and a thermal resistance of 3.5 $m^2 \cdot K/W$ [9], is attached to the rear surface of the lower custom fabricated panels and to one set of the amorphous silicon modules.

The custom made panels were fabricated by a firm that specializes in BIPV panels for commercial and residential applications. Design considerations included incorporating borders that would minimize shading on the cells, the use of readily available cells, and cell interconnections that result in an electrical configuration compatible with the monitoring equipment. A representative panel's cross section is shown in Fig. 3. Individual amorphous silicon cells were not available for incorporation within a custom fabricated panel. Fortunately, commercially available triple-junction amorphous modules were available that could easily be incorporated within the test facility. Each of the two amorphous silicon panels within the test facility consists of two modules. It should be noted that the costs given in Table 1 reflect the fact that the amorphous panels were *off-the-shelf* items whereas the other BIPV panels were custom fabricated.

Instrumentation

Validation of predictive computer simulation tools requires measurement of each building integrated photovoltaic panel's electrical performance and meteorological conditions coincident with the electrical measurements. In addition to these measurements, temperatures associated with each panel and the heat flux through selected panels are measured.

The electrical performance of each building integrated photovoltaic panel is measured using a multi-curve tracer. This instrument continuously operates each panel within 0.2% of its maximum power point [10]. While max power tracking, the multi-tracer is set up to measure, every 15 s, the instantaneous voltage and current from which power is derived. The multi-curve tracer also records the incident irradiance, using a precision spectral radiometer, rear panel temperature, and outdoor ambient temperature as part of the 15 s scans. Every 5 min, the 15 s readings are averaged and saved. In addition to these data, the multi-curve tracer obtains a current versus voltage (IV) trace for each panel

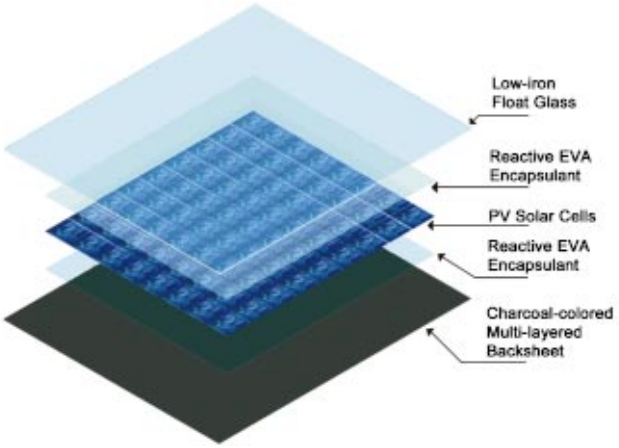

Fig. 3 BIPV Panel Cross Section

Table 1 Building integrated photovoltaic panel specifications

Cell Technology	Single Crystalline	Poly Crystalline	Silicon Film	Triple-Junction Amorphous
Panel Dimensions (m×m)	1.38×1.18	1.38×1.18	1.38×1.18	1.37×1.48
Front Cover	6 mm glass	6 mm glass	6 mm glass	Tefzal
Encapsulant	EVA	EVA	EVA	
Backsheet/Color	Tedlar/Charcoal	Tedlar/Charcoal	Tedlar/Charcoal	Stainless Steel
Cell dimensions (mm×mm)	125×125	125×125	150×150	119×340
Number of Cells (in series)	72	72	56	44
Adjacent Cell Spacing (mm)	2	2	2	
Vertical Border Width (mm)	100	100	51	8
Top Border Height (mm)	72	72	55	11
Bottom Border (mm)	70	70	29	5
Recessed Distance to PV Cell (mm)	12	12	12	9
Glazing Covered by PV Cells %	63	69	80	88
Total Cost ($)	1324	1123	995	578
Price/Watt ($/W)	8.66	8.43	10.75	4.52
Rated Power (W)	153	133	93	128
Cell Area (m^2)	1.020	1.128	1.341	1.780
Aperture Area (m^2)	1.682	1.682	1.682	2.108
Coverage Area (m^2)	1.160	1.160	1.371	1.815

every five minutes when the irradiance is above a minimum threshold of 15 W/m^2. The short circuit current, open circuit voltage, peak power, current at peak power, voltage at peak power, fill factor, and electrical efficiency are automatically computed. Incident irradiance, rear panel temperature, and outdoor temperature are recorded before and after each I-V trace.

One objective of NIST's BIPV Program is to measure the thermal performance of the building integrated photovoltaic panels. This is being done through the use of heat flux transducers attached to selected panels. The resulting measurements will be compared to predicted heat fluxes that would have occurred if conventional building materials were used. The actual heat flux measurements will be the subject of a subsequent publication and are not discussed within this paper. During the design of the test facility, a finite element analysis revealed that the use of heat flux transducers on non-insulated panels could alter the cell temperatures under the heat flux transducer as much as 1°C relative to the surrounding cells. The researchers were concerned that the resulting non-uniform temperature distribution would alter the panel's electrical performance. For this reason, heat flux transducers were only attached to the insulated panels as the thermal resistance of the heat flux transducer is small compared to the thermal insulation. In order to measure the heat flux that occurs through the non-insulated panels, an extra non-insulated panel with an attached heat flux transducer was added to the facility. This panel is identical in construction to the paired single-crystalline BIPV panels, with the exception of its smaller size. The sole purpose of this extra panel is to measure the heat flux through a non-insulated BIPV panel. The electrical measurements from this extra panel will not be used for validating electrical performance algorithms.

Multiple foil-type, type-T thermocouples are installed on each building integrated photovoltaic panel. These sensors are located on the rear of each panel, the rear face of the heat flux transducer (if present), and the rear surface of the attached insulation. During fabrication of the single-crystalline, polycrystalline, and silicon film panels, thermocouples were attached to the rear surface of two cells within each panel. Each temperature sensor was individually calibrated prior to installation.

Predictive simulation tools require meteorological data to predict the electrical performance of building integrated photovoltaic panels. Two meteorological stations, a complete roof top station and a *test bed* meteorological station, are providing this data. The roof top meteorological station incorporates an automated solar tracker and instruments to measure solar radiation, ambient temperature, and wind conditions. The automated solar tracker is a two-axis azimuth/elevation device programmed to align the solar radiation instruments with the normal incidence of the sun. Two pyrheliometers are mounted on the automated solar tracker and are used to measure the solar radiation's beam component. A precision spectral pyranometer and shading disk are also mounted on the automated solar tracker. The shading disk is positioned such that the precision spectral pyranometer on the tracker is continuously shaded, providing a measurement of the solar radiation's diffuse component.

A pair of redundant precision spectral pyranometers, mounted on a horizontal surface near the automated solar tracker, is used to measure global solar radiation. Long-wave radiation, beyond 3 μm, is measured using a precision infrared radiometer. Wind speed and direction are measured using a three-cup anemometer and wind direction sensor. A sheathed type-T thermocouple sensor, enclosed in a naturally ventilated multi-plate radiation shield, is used to measure ambient temperature. The output signals from the meteorological station's instruments are measured using a data acquisition system.

The *test bed* meteorological station consists of two precision spectral pyranometers, one precision infrared radiometer, and two radiatively shielded type-T thermocouples, and an ultrasonic wind sensor. The ultrasonic wind sensor is used to measure the magnitude and direction of air movement over to the panels. All of the instruments are mounted on the building's vertical façade, adjacent to the BIPV panels. This set of meteorological instruments provides data at the actual BIPV site and eliminates and any errors that may arise when attempts are made to predict the radiation on a vertical surface from the horizontal measurements collected from the roof top facility. Additional information on these meteorological stations and the test facilities are provided in Ref. [8].

Experimental Results

Prior to installing the heat flux transducers and thermal insulation, the BIPV panels were monitored to determine if performance differences existed between the two panels of each cell technology. During a 29-day monitoring period (November 9–December 7, 1999) the differences in delivered energy between the two panels of each technology was less than 2.0%. Specifically, the measured differences were (0.7, 1.3, 0.3, and 1.8%) for the single-crystalline, polycrystalline, silicon-film, and amorphous silicon panel sets. The performance differences observed during this initial comparison period were assumed to exist throughout the year and so were used to normalize the results recorded after one of each paired panel was insulated. The expanded uncertainty, using a confidence level of 95%, associated with the energy measurements presented in this paper is $\pm 1.2\%$.

The limited pre-insulation data suggests that custom made BIPV panels can be manufactured without significant differences in panel to panel performance. It is interesting to note that the

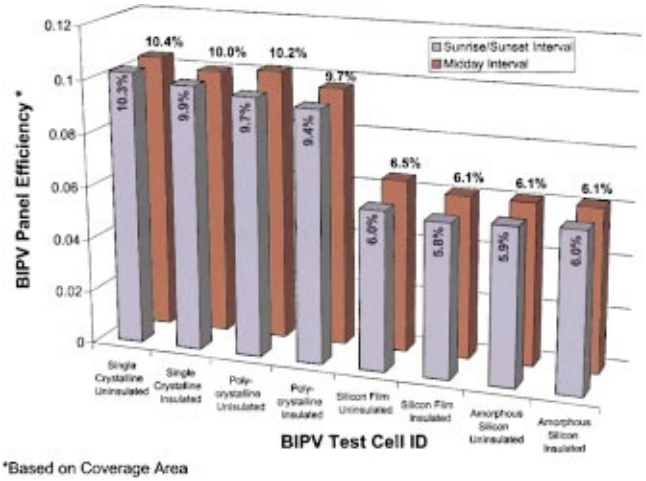

Fig. 4 Overall BIPV Conversion Efficiency

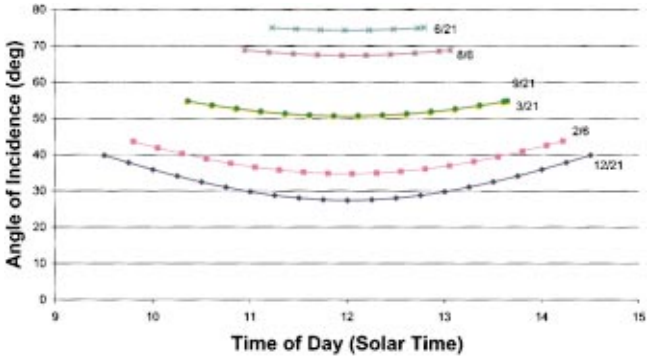

Fig. 5 Midday Time Intervals and Angles of Incidence for Amorphous Silicon Panels

technology with the greatest panel to panel difference is 1.8%, is amorphous silicon. Unlike the other technologies, which were custom manufactured, the amorphous silicon panels represent *off the shelf* modules.

The efficiency of the building integrated photovoltaic panels in converting the incident solar radiation into electrical energy is referred to as the conversion efficiency,

$$\eta_c = \frac{\int_o^\tau P_o d\tau}{A \int_o^\tau H_T d\tau} \tag{1}$$

where

A is a representative area, m^2,
H_T is the incident solar radiation, W/m^2,
P_o is the panels electrical power output, W

and

τ is the time interval selected for monitoring, h.

Unlike other variables in Eq. 1, the selection of an appropriate area is somewhat subjective for the building integrated photovoltaic panels. For example, the area of each cell within a panel times the number of cells yields an area referred to as the cell area. The aperture area is defined as the sunlit opening in the building wall prior to adding the sashing used for mounting the BIPV panels. A third area, referred to in this paper as the coverage area, is defined as the portion of the panel covered by the cells including the areas associated with the spaces between cells. The areas associated with each cell technology are given in Table 1.

Figure 4 gives the overall efficiency of the building integrated photovoltaic panels from January 4 through December 31, 2000. The expanded uncertainty associated with the efficiency results is $\pm 2.4\%$. The coverage area was used to compute the efficiencies in Fig. 4. There are two efficiencies plotted for each building integrated photovoltaic panel in Fig. 4. The bars in the foreground are computed using sunrise to sunset measurements of the incident irradiance and power output. The background bars are the efficiencies of the various panels computed only during the middle of each day when shading along the vertical sides of the panels was not present on any cells within any of the BIPV panels. The panels in which shading is most problematic in this particular installation, and thus acts as a limiting case, are those that utilize the amorphous silicon cells. This is due to the small borders, 8 mm on its vertical sides and 11 mm along the horizontal top edge, that exist between the cells within amorphous silicon panels and the exterior sash that secures the panel, Table 1. The BIPV panels are recessed from the front of the surrounding mullions approximately 6 mm in order to accommodate the exterior retaining sash. Figure 5 shows the hours and the accompanying incident angle during which no shading along the vertical sides of the amorphous silicon panel occurs. This interval, hereafter referred to as the *midday interval*, is one of two data collection intervals—the other being sunrise to sunset—used for analysis in this paper. It is interesting to note that at the summer solstice, June 21, the midday interval (when the cells within amorphous silicon panels are un-shaded along their vertical sides) is less that 2 h and the incident angles during this interval all exceed 70°.

Figure 5 does not account for hours when minimal shading occurs along the upper edge of the amorphous silicon panels. If included, the result is several days bracketing the summer solstice where before the vertical shading stops, the horizontal shading starts, and then in the afternoon, the vertical shading on the opposite side of the panel starts before the horizontal shading ends. For the worst case—solar noon on the summer solstice—the shading on the upper edge of the amorphous silicon panels is 21 mm. Given this relatively minor worst case of upper edge shading on the comparatively large individual amorphous silicon cells, plus the researchers' desire to have middle-of-the-day performance comparisons for every day of the year, the decision to define the time interval in terms of periods of no shading along the vertical sides of the amorphous silicon panels was made. The potential for upper edge shading was considered when designing the custom-made BIPV panels and, as a result, the upper row of cells in the single-crystalline, poly-crystalline, and silicon film panels are never shaded due to the upper, horizontal exterior sash.

The highest overall conversion efficiency (sunrise to sunset) was achieved using single-crystalline cells. The insulated single-crystalline panel efficiency was 3.8% lower than the non-insulated panel, 9.9% versus 10.3%, Fig. 4. The polycrystalline panels differed by 3.1%: 9.7% for the insulated panel compared to 9.4% for the non-insulated panel. The non-insulated and insulated silicon film panels converted 6.0% and 5.8% of the incident solar energy into electrical energy, a 3.3 % difference. Finally, Fig. 4 shows that the addition of insulation to an amorphous silicon panel improved the panels' efficiency from 5.9 % to 6.0 %.

As previously noted, selection of the area used in computing efficiency is somewhat subjective. Figure 6 shows the overall conversion efficiency of the building integrated photovoltaic panels using the three areas previously discussed, cell area, coverage area, and aperture area. The values in Fig. 6 corresponds to the midday interval that was defined above. The relative areas vary depending upon a number of design choices. For example, although the single crystalline and polycrystalline BIPV panels have

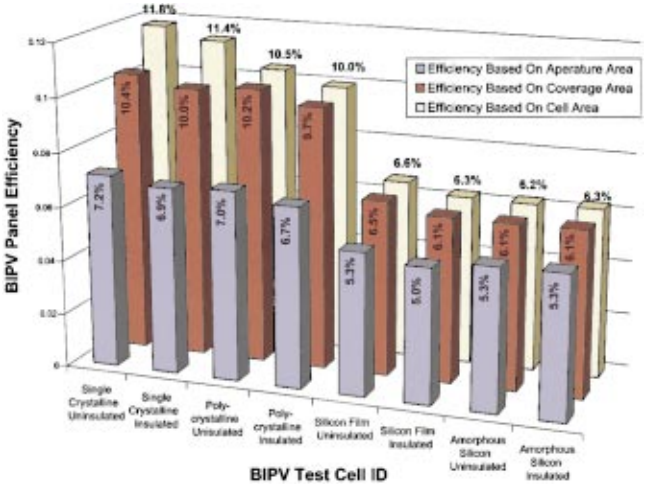

Fig. 6 Overall BIPV Conversion Efficiency-Midday Interval

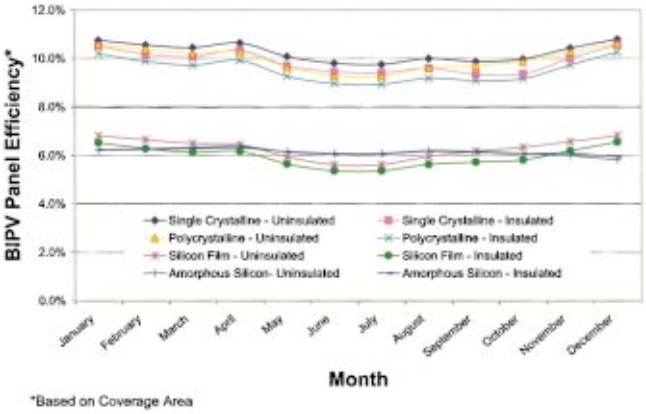

Fig. 8 Monthly BIPV Panel Conversion Efficiency-Midday/ Interval

identical border areas and cell spacing (Table 1), the fact that the single crystalline cells have diagonal rather than square corners results in significantly different efficiencies depending upon which area is used, cell or coverage. In the case of the polycrystalline panels, which utilize square cells, the difference in cell and coverage area efficiencies is small. These results show the clear need to identify the area that is used when presenting efficiency results.

The monthly building integrated photovoltaic conversion for both the insulated and non-insulated panels is shown in Fig. 7. With the exception of the amorphous silicon panels, the highest conversion efficiency was obtained during the month of January. The monthly variation in efficiency is primarily attributed to variations in the incident angle, which varies from 27.4° at solar noon on December 21 to a value of 74.3° at solar noon on June 21. Variations in cell temperatures and shading on the cells due to the surrounding mullions are also responsible, to a lesser extent, for the monthly variations. It is interesting to note that the monthly conversion efficiencies of the amorphous silicon panels are relatively constant from month to month compared to the remaining panels. This behavior is attributed to the fact that amorphous silicon panels are less affected by the angle of incidence relative to the other cell technologies [11].

Figure 8 shows the monthly conversion efficiencies computed using only the data captured during the mid-day intervals. The monthly efficiency of the single-crystalline, polycrystalline, and silicon film panels decreases from January through March in a near linear manner. The amorphous silicon BIPV panel conversion efficiencies slightly increase during this time interval. After April, the efficiencies decline until June. The BIPV panel efficiencies for June and July are almost equivalent. During August all of the efficiencies improved relative to July. The efficiencies decrease slightly in September and, with the exception of the amorphous silicon panels, improve each month through December.

Comparing Figs. 7 and 8, the conversion efficiencies are comparable for the months of January through April, September through December. The greatest differences are observed for the months of May through August. It is believed that these larger differences are due to the greater angles of incident between the BIPV panels and the sun that occurs during the central hours of the days during these months, Fig. 5. Consistent with monthly results previously discussed, the difference in conversion efficiency between the sunrise to sunset results, Fig. 7, and the results for the midday intervals, Fig. 8, is much less significant for the amorphous silicon panels than is exhibited by the other cell technologies.

Further comparison of Figs. 7 and 8 shows that the difference between the insulated and non-insulated panels is more pronounced in Fig. 8. This is a result of the panel operating temperatures. During the midday hours, the difference between the insulated and non-insulated panel temperatures are greater, resulting in a greater performance shift. This phenomenon will be discussed in greater detail when the hourly performance results are presented.

The daily conversion efficiency for a representative month, July 2000, is plotted in Fig. 9. On a daily basis, the differences between the insulated and non-insulated panels for each of the crystalline technologies remain relatively constant except when poor solar conditions exist. During the days in which the incident solar

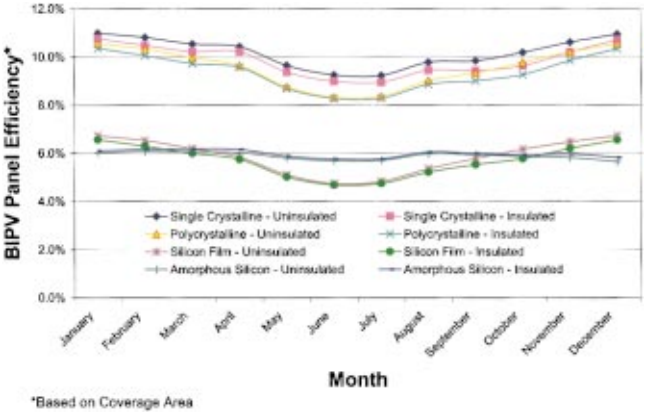

Fig. 7 Monthly BIPV Conversion Efficiency-Sunrise/Sunset

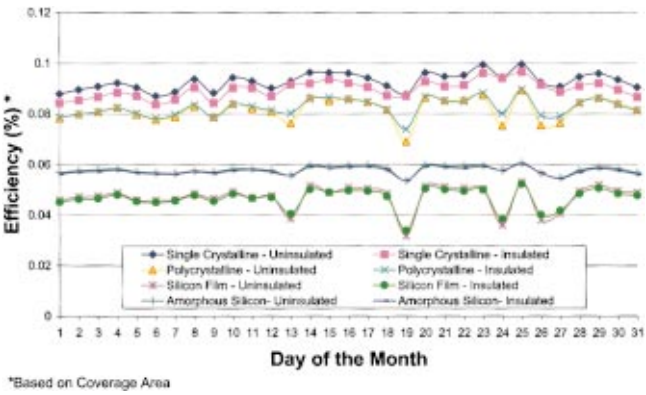

Fig. 9 Daily BIPV Panel Conversion Efficiency-Sunrise/Sunset

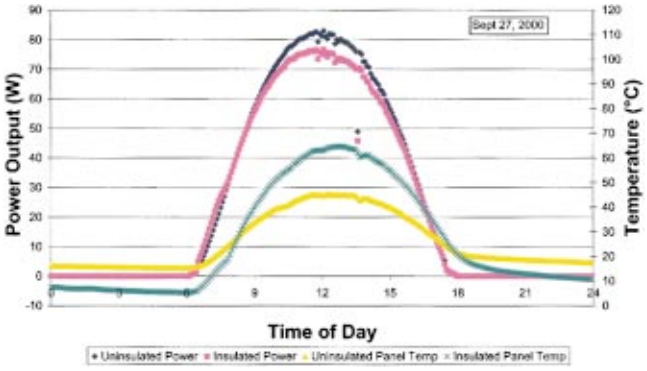

Fig. 10 Single Crystalline Panels-Power Output and Temperature

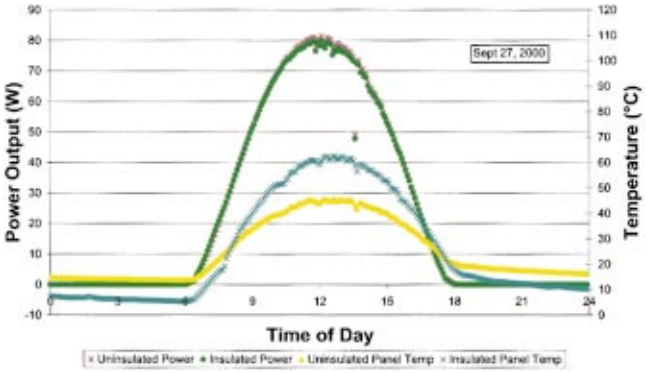

Fig. 11 Amorphous Silicon Panels-Power Output and Temperature

energy was low (July 13, 19, 24, 26, and 27), the difference between the paired single-crystalline panels diminishes, whereas the performance difference for the paired polycrystalline panels increases. The silicon film appears to exhibit the same behavior as the polycrystalline panels but to a lesser extent. There is essentially no difference between the insulated and non-insulated amorphous silicon panels. It is interesting to note the relative performance of the insulated and non-insulated panels for an individual day. Figure 10 shows the insulated single-crystalline and non-insulated single-crystalline cell temperatures for September 27. The expanded uncertainty of the temperature measurements using a confidence level of 95%, is $\pm 0.3°C$. At 12:55, the insulated panel is 19.8°C higher than the non-insulated panel. This was an extremely clear day with the exception of a few minutes around 14:30. The power output of these two modules, also shown in Fig. 10, closely coincide prior to 9:20 and after 16:45. During the central part of the day, the non-insulated panel outperforms the insulated panel. At 12:55 this difference is approximately 9%. The uncertainty associated with the power measurements is $\pm 1.2\%$, assuming a 95% confidence level. For the same day the recorded backside panel temperatures and power outputs for the amorphous silicon panels are plotted in Fig. 11. Although the amorphous panel is 17°C higher at solar noon, the power outputs are essentially identical.

Table 2 summarizes the monthly and cumulative energy production, energy density, operating temperatures, and meteorological conditions for each BIPV panel. The cumulative energy production ranged from a high of 105.4 kW·h for the non-insulated single-crystalline panel to a low of 69.7 kW·h for the insulated silicon film panel. Due to the variations in coverage area, a more meaningful comparison is the energy density. The energy density is computed by dividing the cumulative energy production by the coverage area of each panel. The cumulative energy density

Table 2 Monthly and cumulative BIPV panel performance

		Jan 2000	Feb 2000	Mar 2000	Apr 2000	May 2000	Jun 2000	Jul 2000	Aug 2000	Sep 2000	Oct 2000	Nov 2000	Dec 2000	Total
Panel Energy Production Sunrise to Sunset (Wh)	Single Crystalline—U	11795	12197	12289	6628	6745	6520	7185	7626	10119	14243	10036	11985	105384
	Single Crystalline—I	11556	11833	11925	6491	6552	6332	6967	7367	9694	13463	9644	11725	101827
	Poly Crystalline—U	11332	11662	11624	6130	6124	5859	6509	7029	9596	13668	9653	11546	99187
	Poly Crystalline—I	11116	11349	11341	6084	6075	5833	6452	6904	9262	12956	9317	11327	96688
	Silicon Film - U	8538	8711	8541	4390	4217	3947	4443	4938	7024	10186	7235	8698	72170
	Silicon Film—I	8334	8399	8273	4318	4146	3904	4372	4810	6718	9543	6928	8487	69745
	Amorphous—U	10117	10734	11064	5995	6345	6272	6954	7295	9548	12822	8613	9681	95757
	Amorphous—I	10252	10894	11287	6130	6431	6353	7029	7381	9647	12954	8832	9977	97191
Panel Energy Density* Production Sunrise to Sunset (Wh/m2)	Single Crystalline—U	10171	10518	10597	5715	5816	5622	6195	6576	8726	12282	8654	10334	90871
	Single Crystalline—I	9965	10204	10283	5598	5650	5460	6008	6353	8359	11609	8316	10110	87804
	Poly Crystalline—U	9771	10056	10023	5286	5281	5053	5613	6061	8275	11786	8324	9956	85528
	Poly Crystalline—I	9585	9786	9779	5246	5238	5030	5563	5953	7987	11172	8034	9767	83374
	Silicon Film - U	6226	6353	6228	3201	3076	2878	3240	3601	5122	7429	5276	6343	52631
	Silicon Film—I	6077	6125	6033	3149	3023	2847	3188	3508	4899	6960	5052	6189	50862
	Amorphous—U	5573	5913	6095	3302	3495	3455	3831	4018	5260	7063	4745	5333	52750
	Amorphous—I	5648	6001	6218	3377	3542	3500	3872	4066	5314	7136	4865	5496	53540
Average Backside Panel Temperature Sunrise to Sunset (°C)	Single Crystalline—U	27.0	27.7	26.7	23.7	27.0	28.7	29.6	30.9	31.7	32.9	30.0	26.9	28.7
	Single Crystalline—I	28.8	31.0	29.0	24.2	29.9	31.9	33.2	35.1	37.4	40.3	35.6	28.7	32.2
	Poly Crystalline—U	26.9	27.7	26.7	23.8	27.1	28.8	29.7	31.0	31.8	33.0	30.1	26.8	28.7
	Poly Crystalline—I	28.3	30.5	28.8	24.0	29.7	31.8	33.0	34.9	37.1	39.9	35.0	28.1	31.9
	Silicon Film - U	27.4	28.1	27.1	23.8	27.3	29.0	29.9	31.3	32.2	33.6	30.6	27.3	29.0
	Silicon Film—I	29.1	31.0	29.4	24.2	30.0	32.0	33.3	35.2	37.5	40.4	35.5	28.8	32.3
	Amorphous—U	23.3	24.8	24.9	22.5	26.5	28.5	29.2	30.3	30.7	31.1	27.2	23.3	26.9
	Amorphous—I	23.7	26.5	26.4	22.2	28.3	30.7	32.0	33.6	34.9	37.0	30.8	23.8	29.3
Average Outdoor Ambient Temp (°C)**		3.5	8.5	13.2	17.2	21.5	24.8	24.9	25.3	22.1	18.9	11.2	2.6	16.1
Average Indoor Ambient Temp (°C)**		21.9	22.0	22.2	22.2	23.4	24.5	24.9	25.6	25.0	23.8	22.1	20.5	23.2
Vertical Solar Insolation (Wh/m2)**		92563	97282	100528	54806	60274	60742	67132	67241	88704	120599	81580	94485	985939
Complete Days of BIPV Electrical Performance Data (days)		28	29	31	23	28	30	31	29	27	31	26	31	344
Average Daily Insolation (Wh/m2)		3306	3355	3243	2383	2153	2025	2166	2319	3285	3890	3138	3048	2866

*Based on coverage area
**Evaluated using data collected between sunrise and sunset
U denotes Uninsulated.
I denotes Insulated.

ranged from a high of 90.9 $kW \cdot h/m^2$ for the non-insulated crystalline panel to a low of 50.8 $kW \cdot h/m^2$ for the insulated silicon film panel.

The addition of insulation to the rear of crystalline, polycrystalline, and silicon film panels resulted in declines in energy production of 3.3, 2.5, and 3.4%, respectively. Unlike the other BIPV panels, the insulated amorphous silicon panel outperformed the non-insulated panel by 1.5%. The results in Table 2 show that for a south-facing vertical façade at the latitude of the test-bed, 39.1°, BIPV energy production will be at its greatest magnitude during the winter months.

Summary

Among the barriers to the widespread proliferation of building integrated photovoltaics is the lack of performance data and validated performance models. A building integrated photovoltaic *test bed* has been constructed that will address these barriers. The facility, placed into operation in January 2000, is capable of providing side-by-side performance comparisons of up to eight panels.

Eight BIPV panels are currently installed within the *test bed*. The panels include custom fabricated single-crystalline, polycrystalline, and silicon film panels as well as commercially available amorphous silicon modules. An insulated and non-insulated panel of each cell technology is installed. This paper contains the first twelve months of performance results, January through December, collected at NIST's BIPV *test bed*.

The selection of the area used to compute efficiency is subjective and can have a dramatic impact on reported results. The potential BIPV system owner must take great care in using a consistent area when comparing BIPV conversion efficiencies. Three areas are discussed in this paper: cell, coverage, and aperture. Unlike cell area, which is fixed by the cell's manufacturer, and aperture area, which is dependent upon the building's design, the coverage area can vary significantly dependent upon the panel's design. For example, an architect may elect to use large spaces between cells and transparent materials in the BIPV's panel construction to provide day-lighting as well as electrical power. The variation in reported efficiency resulting from area selection can be tremendous. The conversion efficiency of the non-insulated single-crystalline panel in this study could be reported as (7.2, 10.4, or 11.8%), as a result of using the aperture, coverage, or cell area in computing efficiency.

During the twelve months that the panels have been monitored, the measured midday efficiencies for the non-insulated panels are (10.4, 10.2, 6.5, and 6.1%) for the single-crystalline, polycrystalline, silicon film, and amorphous silicon panels, respectively. The non-insulated single-crystalline, polycrystalline, and silicon-film panels outperformed the insulated panels. The midday performance differential was 3.8% for the single-crystalline, 4.9% for the polycrystalline panels, and 6.1% for the panels constructed using silicon film. By comparison, the insulated amorphous silicon panel conversion efficiency was identical to the paired uninsulated panel.

The single-crystalline, polycrystalline, and silicon film panels were most efficient during January and least efficient during the months of June and July. The month-to-month variation in efficiency is attributed primarily to the large variations in incident angle. The incident angle between the sun and BIPV panels varied from a low of 27.4° on December 21 to 74.3° on June 21 for these vertical south-facing panels. Placement of the panels on a horizontal roof would have resulted in incident angles of 62.6° and 15.7°, respectively, on these dates.

The data summarized in this paper should be of interest to building owners, photovoltaic cell manufacturers, and fabricators of BIPV panels. In subsequent publications [12], the hourly data will be compared to the computer predictions.

Acknowledgment

The authors would like to acknowledge Gerald Ceasar of NIST's Advanced Technology Premium Power Program and the California Energy Commission for providing financial support for this project. Also recognized for their contributions are Jake Brown of Solar Building Systems for his assistance in the design and fabrication of the BIPV panels. Gratitude is extended to the following NIST personnel who have assisted the authors: Stanley T. Morehouse for his role in fabricating the various facilities described within this paper; Robert Zarr for calibrating the heat flux transducers, Daniel Vennetti for calibrating the various instruments associated with the BIPV facility and preparing the graphics; Michael Christopher, along with Daniel Vennetti, for transforming the experimental data generated by the BIPV *test-bed* into useful formats; and Paula Svincek for manuscript preparation.

References

[1] Cook, G., David, R., Gwinner, D., and Hicks, A., 2000, *Photovoltaics; Energy for the New Millennium*, 1-17, 1-1-2000, NREL, Golden, CO, Department of Energy.
[2] Schoen, T. J., 1999, ''Information,'' *Renewable Energy World*, 2, No. 5, p. 84.
[3] King, D. L., Dudley, J. K, and Byoson, W. E., 1997, ''PVSIM: A Simulation Program for Photovoltaic Cells, Modules, and Arrays,'' *Proc. of 26th IEEE Photovoltaics Specialists Conf*., Anaheim, CA.
[4] 1999, Photovoltaic Analysis and TrAnsient Simulation Method (PHANTASM), Building Integrated Photovoltaic Simulation Software, Solar Energy Laboratory, University of Wisconsin, Madison, WI.
[5] ENERGY-10, V1.3, 2000, ''A Tool for Designing Low Energy Buildings,'' Sustainable Buildings Energy Council, Washington, D.C.
[6] IV Curve Tracer, Solar Design Studio, v4.0, Maui Solar Energy Software Corp., Haiku, I, October 2000.
[7] King, D. L., 1997, ''Photovoltaic Module and Array Performance Characterization methods for all System Operating Conditions,'' *Proc. of NREL/SNL Photovoltaics Program Review Meeting*, Nov. 1996, Lakewood, CO, AIP Press, New York.
[8] Fanney, A. H., and Dougherty, B. P., 2000, ''Building Integrated Photovoltaic Test Facility,'' *Proc. of Solar 2000: Solar Powers Life, Share the Energy*, June, Madison, WI, ASME, New York.
[9] NIST R-Matic Test Report R000420 B, April 20, 2000.
[10] Raydec, 1988, ''Photovoltaic Operations and Maintenance Manual,'' Ver. 4.0.
[11] King, D. L, Kratochvil, J. A., and Boyson, W. E., 1997, ''Measuring Solar Spectral and Angle-of-Incidence Effects on Photovoltaic Modules and Solar Irradiance Sensors,'' *26th IEEE Photovoltaic Specialists Conf.*, Anaheim, CA.
[12] Davis, M. W., Fanney, A. H., and Dougherty, B. P., 2001 ''Prediction of Building Integrated Photovoltaic Cell Temperatures,'' *Proc. of Forum 2001, Solar Energy: The Power to Choose*, April 2001, ASES, Washington, DC.